# Structural and Electronic Properties of Cubic $CeO_2$: Unpaired Electrons in $CeO_2$

**CARLOS QUINTANAR,[1] REYNA CABALLERO,[1] JORGE BARRETO,[2] ELIZABETH CHAVIRA,[3] ERNESTO E. MARINERO[4]**

[1]*Facultad de Ciencias, Universidad Nacional Autónoma de México, Ciudad Universitaria, 04510 México D.F., México*

[2]*Instituto de Física, Universidad Nacional Autónoma de México, Ciudad Universitaria, 04510 México D.F., México*

[3]*Instituto de Investigaciones en Materiales, Universidad Nacional Autónoma de México, AP 70-360, 04510 México D. F., México*

[4]*Hitachi San Jose Research Laboratory, 3403 Yerba Buena Road, San Jose, CA 95135*

*Received 30 April 2010; accepted 1 June 2010*
*Published online 18 August 2010 in Wiley Online Library (wileyonlinelibrary.com).*
*DOI 10.1002/qua.22874*

**ABSTRACT:** The high performance of cerium dioxide ($CeO_2$) as support for Au in catalysis relies on its ability to anchor Au clusters and transfer charge to the gold nanoparticles. These two processes are governed by oxygen vacancy formation. To study the localization and the mobility of the electrons left behind by the vacancy from the relaxed oxygen, an experimental and theoretical study is hereby reported. $CeO_2$ powder was synthesized by the polyacrylamide gel method and its microstructure was characterized by X-ray diffraction and high resolution scanning electron microscopy. We have determined the presence of only the fluorite cubic phase in our samples and the formation of acicular particles of $\sim$1 $\mu$m in length. In the electron spin resonance study, we observed that the unpaired electrons are quasi free. A single-line paramagnetic signal is observed that exhibits spin characteristics with a *g*-value of 2.0039 at room temperature. This compares well to the value of 2.0023 determined for free electrons. In addition, we have conducted a theoretical study using a density functional theory cluster approach and calculate the electron spin density of $CeO_2$ clusters. We find that spin density clouds are localized around the cerium ions.  Int J Quantum Chem 110: 2949–2954, 2010

**Key words:** $CeO_2$; oxygen vacancies; electron spin resonance; density functional theory

*Correspondence to:* C. Quintanar; e-mail: cqs@matrix.super.unam.mx

Contract grant sponsor: PAPIIT-UNAM IN113509-3.
Contract grant sponsor: IMPULSA-PUNTA-UNAM.
Contract grant sponsor: CONACyT 80380.

## Introduction

Cerium dioxide ($CeO_2$) having a cubic fluorite crystal structure has been used in catalytic reactions as a reducible oxide support material in emission control catalysis [1, 2]. For achieving high catalytic activity, reducible supports usually exhibit appreciably better performance than nonreducible ones [1]. In the oxidation of CO catalyzed at the surface of metal particles like Au, $CeO_2$ plays an important role [2, 3], and it has been reported that $Au/CeO_2$ catalysts also show high catalytic activity for low-temperature water shift reaction and CO oxidation [4–7].

$CeO_2$ surface defects such as oxygen vacancies have also recently attracted interest because the role they may play in catalytic processes of the CO oxidation [8]. This is attributed to the fact that in metal oxides, point defects such as oxygen vacancies may anchor the metal particles and transfer charge to the metal nanoparticles [9–13]. It has been reported that the electrons left behind by the relaxed oxygen from the vacancy are localized at the cerium ions [14].

This work aims to determine the sites where the electrons left behind by the removal of neutral oxygen from the oxygen site become localized, and whether they weakly or strongly bond to the lattice ions.

To generate defects in our synthesized $CeO_2$ particles, we utilize heat treatment of the powder to produce point defects such as oxygen vacancies. It is known that on annealing the cerium ion reduces from $Ce^{4+}$ to $Ce^{3+}$. We note that according to Freund and coworkers [12], point defects, such as oxygen vacancies, are the most important type of defects that increment the system's catalytic activity. These defects are known to anchor gold particles [11, 12], to enhance the catalytic activity of the metal nanoparticles [12], and to the release of electrons [7]. Using spin density calculations in this work, we have determined the site where the unpaired electrons might be localized, and using spin resonance measurements, we establish the strength of the electron bonding that are released from the vacancies.

## Methods

### SAMPLE PREPARATION

$CeO_2$ mesoparticles were prepared using a modified acrylamide sol–gel technique. This is particularly useful, since the polyacrylamide network inhibits the aggregation of $CeO_2$ particles [15]. Cerium oxide (99.999%, Aldrich) was dissolved in a solution of distilled water at 80°C using oxygenated water (20% vol.) and nitric acid (69–70%, J. Baker), buffered at neutral pH with ammonium hydroxide (28–30%, J. T. Baker), followed by the addition of *N*,*N*′-methylene-bisacrylamide (99.5%, Fluka) and acrylamide (99%, Fluka). The polymerization took place within 4 s resulting in a homogeneous gel. The gel was dried at room temperature in air, pulverized and then heated up to 600°C, and maintained at that temperature for 15 min. Following these procedures, two different subsequent additional treatments are used: in the first one, samples were brought slowly down to room temperature, while in the second procedure, the sample was quenched from 600 to −60°C. For the quenching, a metal copper plate attached to a metal rod was used. The rod was in contact with liquid nitrogen, and once equilibrium was achieved, the temperature at the plate was measured to be −60°C.

Powder X-ray diffraction (XRD) analysis was used to determine the crystalline structure and the residual polymer material present in the samples using a Bruker D8 Advance diffractometer with Cu $K_\alpha$ radiation ($\lambda = 1.5406$ Å), 40 KV and 30 mA equipped with a graphite diffracted beam monochromator. Diffraction patterns were collected at room temperature over the 2θ range 5–140°. The microstructure and morphology were observed by scanning electron microscopy (SEM) analysis using a Zeiss 1540 XB. Electron spin resonance (ESR) measurements were performed using a JEOL JES-RE3X spectrometer, using a cylindrical cavity (TE011 mode) operating at X-band frequencies (near 9.1024 GHz) with 100-kHz field modulation. The *g*-values were obtained by measuring the resonance field using an NMR gaussmeter, JEOL ES-FC5 in combination with a HP-5350 frequency counter. A sample of MgO: $Mn^{2+}$ was used as a standard field marker for ESR measurements. Quartz tubes (2.5 mm ID, 13 mm high) were used for the ESR studies.

## Quantum Chemical Methods

All calculations were performed with the linear combination of Gaussian-type orbitals Kohn-Sham density functional theory (DFT) code deMon2k

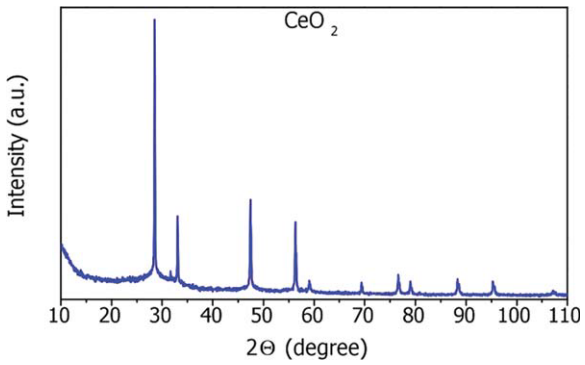


**FIGURE 1.** XRD of a $CeO_2$ sample that was slowly cooled down to room temperature. The spectrum corresponds to the fluorite phase structure. [Color figure can be viewed in the online issue, which is available at wileyonlinelibrary.com.]

[16]. To avoid the calculation of four-center electron repulsion integrals, the variational fitting of the Coulomb potential [17–19] was used. The auxiliary density [20] was expanded in primitive Hermite Gaussian functions and the Perdew, Burke, and Enzerhof generalized gradient approximation [21] was used. The exchange-correlation potential was calculated by numerical integration on an adaptive grid [22, 23] from the auxiliary function density [20]. All electrons of oxygen were treated explicitly using the double-z valence plus polarization basis sets (621/41/1*). For the cerium atoms, the relativistic effective core potential with 19 valence electrons proposed by Schwerdtfeger et al. [24] was used. The GEN-A2 auxiliary function set for the O atoms and the GEN-A2* set for the Ce atoms were used.

## Results and Discussion

### X-RAY DIFFRACTION AND SCANNING ELECTRON MICROSCOPY

Figure 1 shows an XRD spectrum of a $CeO_2$ sample that was slowly cooled down to room temperature. The spectrum reveals sharp reflections that evidence a crystalline phase as well as a background that corresponds to the residual polymer material present in the samples. We note that the spectra corresponding to the fast quenched sample are virtually identical to the one shown in Figure 1 but exhibit even sharper peaks than for the slowly cooled down sample. Spectral analysis of the diffraction pattern indicates that it corresponds to the powder diffraction file 34-0394, associated with a cubic unit cell and a lattice parameter $a = 5.4113$ Å with space group: Fm3m. As can be seen in the spectrum shown in Figure 1, the full width at half maximun (FHWM) of the spectral lines are quite narrow, indicating that the sample is comprised of rather large mesoparticles. This observation is substantiated by the scanning electron microscope (SEM) micrographs obtained and shown in Figure 2. The presence of large crystallites and of elongated "needles" is readily observed. Figure 2 corresponds to a $CeO_2$ xerogel heated at 600°C and slowly cooled down. In this image, acicular $CeO_2$ structures are readily observed. These needles have different lengths: the one on the right side is 0.8 $\mu$m long, whereas the one in the middle of the image is 1.1 $\mu$m in length and the one on the left side of the image is 1.4 $\mu$m long. Also, in the figure, the presence of residual polymer material can be observed and this is highlighted on the upper left portion of the micrograph. It is noted that annealing at 600°C for 15 min is not sufficient to fully decompose and volatize the polymer to produce only particles of the $CeO_2$ compound.

### ESR MEASUREMENTS

Cerium has the [Xe] $4f^2 5d^0 6s^2$ electronic configuration. In the $CeO_2$ fluorite phase, it exhibits a +4 oxidation state [25], $Ce^{4+}$ and $O^{-2}$ ions having

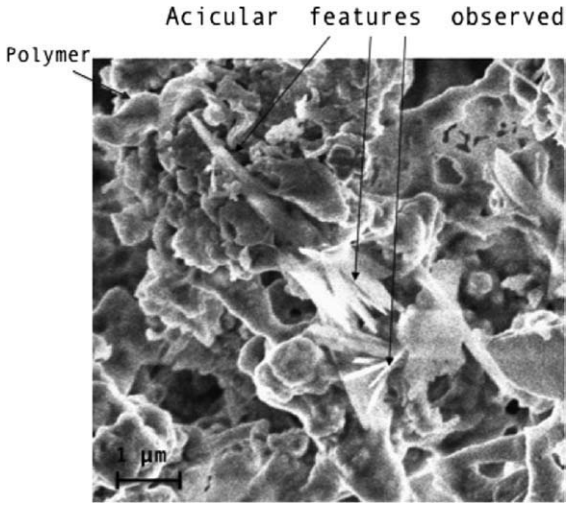


**FIGURE 2.** SEM image showing particle clusters of $CeO_2$ with acicular structures. Some characteristics dimensions are given: the one on the right side is ~0.8 $\mu$m long, the one in the middle ~1.1 $\mu$m, and the one on the left ~1.4 $\mu$m. In the upper left side of the micrograph, an arrow points to the residual polymer.

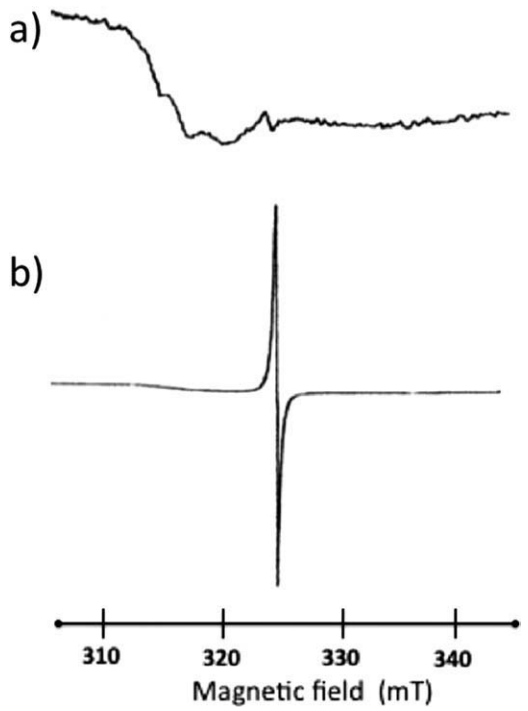


**FIGURE 3.** Electron spin resonance spectrum of both the nonquenched (a) and the quenched (b) $CeO_2$ samples. The spectrum of (a) is amplified 200 times more than that of (b). A $g$ value $= 2.0039 \pm 0.0008$ is determined from these measurements (see text).

closed shells, with the electronic structure of Xenon and Neon, respectively. The presence of oxygen vacancies in $CeO_2$ is suggested to induce the reduction of Ce from 4+ to 3+ to maintain electrostatic balance [25]. In the nonreduced case (closed shells), one should not observe a paramagnetic signal, while in the reduced case, the signal due to the $Ce^{3+}$ is difficult to be observed because of spin lattice relaxation, and only near 4 K can a paramagnetic signal be observed [26]. However, in reports found in the literature, a narrow signal has been observed in EPR spectra of $CeO_2$-based materials yielding $g$-values near the free electron value $g = 2.0023$. This signal has a small linewidth and is readily detected, Gideoni and Stainberg [27] assign this signal to quasi-free electrons or to electrons trapped at oxygen vacancies of the $CeO_2$ lattice. This signal is correlated with the level of defects in the samples [26], thereby suggesting that both facts are intimately related [26]. Therefore, in the most pure and partially reduced $CeO_2$ samples, this signal has a very low intensity [28] or is even absent [29]. Besides, its intensity does not correlate with the degree of reduction of the samples [26].

We performed ESR measurements on two $CeO_2$ samples with different postsynthesis cooling treatments. One was heated up to 600°C and then was let to cool down to room temperature in air. The spectrum is shown in Figure 3(a), the other sample was also heated up to 600°C and then it was quenched to −60°C. The corresponding spectrum for the latter sample is shown in Figure 3(b). Both $CeO_2$ samples show only a paramagnetic line that exhibits free spin characteristics with a $g$-value of 2.0039 with an error of ±0.0008 at room temperature, when compared with the value of 2.0023 for free electrons. Only one ESR transition was observed in both cases, but the line of the quenched sample shown in Figure 3(b) has an intensity which is three orders of magnitude larger than that of nonquenched sample [Fig. 3(a)]. This might indicate that the quenching freezes the mesoparticle defects by hindering their mobility due to the drastically reduced time × temperature product that controls diffusive processes. Therefore, we suggest that the quenching leads to the formation of more quasi-free electrons in the sample.

We exclude the possibility that the ESR signal may be due to the residual polymer material on two grounds: (1) the amount of the residual polymer is the same for both the quenched and slow cooled down samples. (2) the residual polymer is amorphous (no crystalline diffraction peaks besides those corresponding to crystalline $CeO_2$ are present in the XRD spectra). Thus, defects in low concentration should not be expelled from the polymer, as they are from $CeO_2$ crystals bulk, because defects have more sites to localize in a amorphous polymer than in a crystal; therefore, the entropy gain that provides the driving force to expel the defects outside the material is less in amorphous polymers than in crystals, and also the polymer viscosity works against the force that expels defects. Therefore, if there was a contribution to the ESR signal from the polymer, it should have the same contribution in both sample sets, which is contrary to the experimental results. Therefore, we attribute defects in the $CeO_2$ polycrystals as being responsible for the ESR signal that strongly increase as a consequence of the quenching treatment.

## ISO-SPIN DENSITY DFT STUDY

To find out where the unpaired electrons may be localized, a theoretical study was conducted

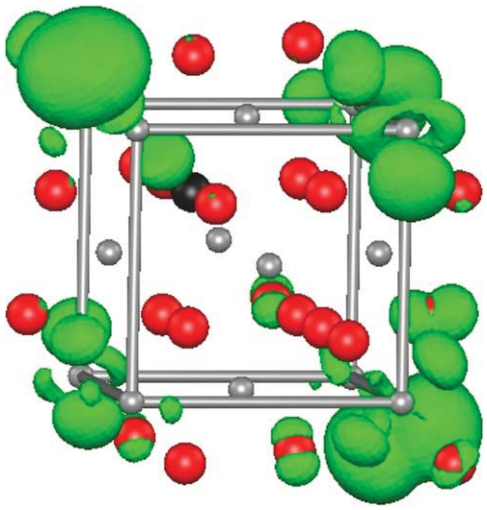

**FIGURE 4.** Spin density calculation of the cluster of the $CeO_2$. The gray and red spheres represent the Ce and O ions, respectively. The vacancy site is indicated by a black sphere. The Ce ions form a face-centered cubic lattice; a cube with an additional ion in the center of each square face. Green surfaces are spin density isosurfaces, they localize around the Ce ions, although some spin density can be observed near the vacancy. [Color figure can be viewed in the online issue, which is available at wileyonlinelibrary.com.]

using a DFT cluster approach. Our cluster has 14 cerium ions and 27 oxygen ions, and one vacancy. In this system, an oxygen ion was removed. The total cluster charge was set to +1 to model a partial compensation of the charge, and we calculated the spin density of this system and is shown in Figure 4. In this figure, the cerium and oxygen ions are represented by gray and red spheres, respectively. The vacancy is represented by a black sphere. In Figure 4, one can observe the face-centered cubic lattice formed by the $Ce^{4+}$ ions (gray spheres), one can see five $Ce^{4+}$ on top of the cube, four in the middle of the cube, and five $Ce^{4+}$ at the bottom of the cube. The spin density is illustrated in green, and one can see that the green clouds are localized around the $Ce^{4+}$ ions. This may be understood considering that Ce is 4+ while the vacancy is only 2+. Our results agree with the results of Esch et al. [14] who reported that the electrons are localized around the cerium ions. Conesa et al. [26] proposed that the quasi-free electrons are conduction electrons or electrons trapped in an oxygen vacancy. Our results are suggestive that the quasi-free electrons may be the conduction electrons, but we do not observe in our theoretical calculations an electron spin density trapped at the vacancy, although as seen in Figure 4. Near the vacancy (black sphere), there exists some net spin density.

## Conclusions

In summary, we have synthesized $CeO_2$ mesoparticles using a modified acrylamide sol–gel technique. The microstructure of the $CeO_2$ particles is the cubic fluorite phase and their morphology exhibits acicular—needle like—elongated crystallites. Defects are generated in the mesoparticles by thermal annealing at 600°C. The diffusivity of the defects is severely hindered by quenching the samples from 600 to −60°C. ESR measurements reveal the presence of a strong paramagnetic signal for said quenched samples that we attribute to the presence of almost-free electrons. Said signal is three orders of magnitude weaker in specimens cooled down slowly from 600°C down to room temperature. To identify the atomic sites where the unpaired electrons originating from trapped defects in the lattice structure, may be localized, a theoretical study was conducted using a DFT cluster approach. We conclude from our spin density DFT cluster studies that the unpaired electrons are localized around the $Ce^{4+}$ ions.

### ACKNOWLEDGMENTS

We thank to Antonio Morales Espino, IF-UNAM and Letícia Baños, IIM-UNAM for their technical support in the X-ray diffraction and EPR measurements. We also thank Vijay Rawat, Hitachi San Jose Research Center, for acquiring the SEM images.

## References

1. Delannoy, L.; Weiher, N.; Tsapatsaris, N.; Beesley, A. M.; Nchari, L.; Schroeder, S. L. M.; Louis, C. Top Catal 2007, 44, 263.
2. Xiao, W.; Guo, Q.; Wang, E. G. Chem Phys Lett 2003, 368, 527.
3. Crucq, A. Catalysis and Automotive Pollution Control III; Elsevier: Amsterdam, 1991.
4. Fu, Q.; Weber, A.; Flytzani-Stephanopoulos, M. Catal Lett 2001, 77, 87.
5. Sakurai, H.; Akida, T.; Tsubota, S.; Kiuchi, M.; Haruta, M. Appl Catal A 2005, 291, 179.

6. Akita, T.; Okumura, M.; Tanaka, K.; Kohyama, M.; Haruta, M. Cat Today 2006, 117, 62.
7. Carretin, S.; Concepcion, P.; Corma, A.; Nieto, J. M. L.; Puentes, V. F. Angew Chem Int Ed 2004, 43, 2538.
8. Li, H.-Y.; Wang, H.-F.; Gong, X.-Q. Phys Rev B 2001, 79, 193401.
9. Abbet, S.; Sanchez, A.; Heiz, U.; Schneider, W. D.; Ferrari, A. M.; Pacchioni, G.; Rosch, N. J Am Chem Soc 2000, 122, 3453.
10. Giordano, L.; Di Valentin, C.; Goniakowski, J.; Pacchioni, G. Phys Rev Lett 2004, 92, 096105.
11. Caballero, R.; Quintanar, C.; Köster, A. M.; Khanna, S. N.; Reveles, J. U. J Phys Chem C 2008, 112, 14919.
12. Baron, M.; Bondarchuk, O.; Stacchiola, D.; Shaikhudinov, S.; Freund, H.-J. J Phys Chem 2009, 113, 6042.
13. Carrasco, J.; Lopez, N.; Illas, F.; Freund, H.-J. J Chem Phys 2006, 125, 074711.
14. Esch, F.; Fabris, S.; Zhou, L.; Montini, T.; Africh, C.; Fornasiero, P.; Comelli, G.; Rosei, R. Science 2005, 309, 752.
15. Wang, H.; Gao, L.; Li, W.; Li, Q. Nanostruct Mater 1999, 11, 1263.
16. Köster, A. M.; Calaminici, P.; Casida, M. E.; Flores-Moreno, R.; Geudtner, G.; Goursot, A.; Heine, T.; Ipatov, A.; Janetzko, F.; del Campo, J. M.; Patchkovskii, S.; Reveles, J. U.; Salahub, D. R.; Vela, A. deMon2k V. 2.1.8, The international deMon developers community. Available at: http://www.deMon-software.com, 2006.
17. Dunlap, B. I.; Connolly, J. W. D.; Sabin, J. R. J Chem Phys 1979, 71, 4993.
18. Mintmire, J. W.; Dunlap, B. I. Phys Rev A 1982, 25, 88.
19. Mintmire, J. W.; Sabin, J. R.; Trickey, S. B. Phys Rev B 1982, 26, 1743.
20. Köster, A. M.; Reveles, J. U.; del Campo, J. M. J Chem Phys 2004, 121, 3417.
21. Perdew, J. P.; Burke, K.; Ernzerhof, M. Phys Rev Lett 1996, 77, 3865.
22. Krack, M.; Köster, A. M. J Chem Phys 1996, 108, 3226.
23. Köster, A. M.; Flores-Moreno, R.; Reveles, J. U. J Chem Phys 2004, 121, 681.
24. Schwerdtfeger, P.; Dolg, M.; Schwarz, W. H. E.; Bowmaker, G. A.; Boyd, P. D. W. J Chem Phys 1989, 91, 1762.
25. Trovarelli, A. In Structural Properties and Nonstoichiomerict Behavior of $CeO_2$ Catalysis By Ceria and Related Materials 2; Alessandro Trovarelli, Ed.; World Scientific Publishing Co. Pte. Ltd. London: 2002, p 15.
26. Conesa, J. C.; Fernadez-Garcia, M.; Martinez-Arias, A. Studies of Ceria-Containing Catalysts Using Magnetic Resonance and X-Ray Based Spectroscopies, Catalysis By Ceria and Related Materials 2; Alessandro Trovarelli, Ed.; World Scientific Publishing Co. Pte. Ltd.: London, 2002, p 169.
27. Gideoni, M.; Stainberg, M. J Sol St Chem 1972, 4, 370.
28. Soria, J.; Martínez-Arias, A.; Conesa, J. C. J Chem Soc Faraday Trans 1995, 91, 1669.
29. Zhang, X.; Klabunde, K. J. J Inorg Chem 1992, 31, 1706.